Oak glulam bending strength by XFEM simulation including stochastic and autocorrelated board properties

CRISTÓBAL TAPIA CAMÚ, SIMON AICHER

MPA Universität Stuttgart

Abstract: The paper reports on the simulation of load capacity enhanced bending strength of glued laminated timber (GLT) beams made of oak (Querqus robur, Q. petraea) wood. Hardwoods, such as oak and beech, gained increasing attention in recent years with regard to structural applications due to superior mechanical properties and changes of forestry plantation policy, shifting the forest stock towards hardwoods. A significant increase to a wider use of hardwood GLTs at present is hindered by the fact that the current European GLT standard is restricted to softwoods, due to several hardwood inherent material and bonding features. Within a recent European research project, a major task contributed by MPA University of Stuttgart consisted in the development of a finite element model for the derivation of hardwood GLT bending capacities. On the consideration of existing finite element models, combined with Montecarlo-based stochastically generated input parameters, an advanced calculation model based on XFEM was derived. The method is especially capable to simulate the crack evolution and strain softening in heterogeneous materials. The new hardwood glulam model incorporates different fracture energies for wood and finger joints, allows for yielding in the compression zone and accounts for the variation of the modulus of elasticity, described by an autoregressive process, along the board's length. The model was verified with an extensive dataset of board's strength and stiffness properties and full-sized beam test results, obtained in the frame of a former ETA test campaign on oak glulam. The presented results of the XFEM model are in very good agreement with the beam test results and predict the size effect in an accurate manner. Further simulation runs with the model, based on different input values for boards, finger joints and calibration data for beams will enable a parametric closed-form hardwood glulam bending strength equation similar to the present EN 14080 solution for softwood glulams.

1. Introduction

The use of hardwoods, especially of oak and beech, as a structural material in the building sector has gained considered importance in Europe. Major reasons herefore are i) extensive over-aging hardwood forest stands which so far are not economically used, ii) architectural aspects and iii) the recognized higher strength and stiffness properties as compared to softwoods, which can be significant. The supply of hardwoods in Germany will further increase in the coming decades considerably,

due to a change in forestry plantation policy, favoring hardwoods at many locations due to better aptness for the respective soil and climate conditions. Similar to softwoods, but even increased due to growth specific characteristics, the advantages of the mechanical properties of hardwoods can only be utilized efficiently when processed to engineered wood products, such as the beam-type product glued laminated timber (glulam) or the plate-type materials cross-laminated timber (CLT) and laminated veneer lumber (LVL). Here exclusively glulam made of oak (Querqus robur, Q. petraea) is regarded.

Oak in the form of solid wood has a long and impressive history in house construction, especially in half-timbered houses and heavy roof structures in medieval times until late 18th century. The oak glulam roof structure of the new Scottish parliament in Edinburgh, inaugurated in 2004, is one of several outstanding proofs of the revival of the material in engineering format.

Currently, the European glulam standard EN 14080 [1] covers exclusively specifications, requirements and evaluation of conformity procedures for glulam made of softwoods. The standard includes a bending strength model for homogeneous glulam based on the characteristic values of the mechanical properties – tension strength of the boards and bending or tension strength of finger joints. Inhomogeneous build-ups with different strength classes of the boards are then captured by beam theory and transformed sections.

Since the wood and finger joint properties of hardwood species can differ from softwoods significantly, a direct application of the existing strength model to glulam made of hardwoods is generally not possible. Hence, today hardwood glulams are brought on the market and used in structural applications on the basis of national technical approvals or European Technical assessments. All present technical specifications for oak glulam [2], [3] as for chestnut glulam [4] are based on a large number of costly tests. A first analytical hardwood glulam model based on Weibull theory (Aicher and Stapf [5]) is well suited for build-ups where the load capacity is overly-dominated by finger joint strength. However, as it does not incorporate the lamination effect, the model is limited to a specific class of hardwood glulams.

In order to enable hardwood glulams an easier access to the building market one of the major aims of the European research project „EU Hardwoods for the building sector" in the frame of the European WoodWisdom agenda (www.eu-hardwoods.eu) consisted in the development of a generally applicable computational (FEM) model for these products. Based on the model, accompanied by experimental verifications an analytical bending strength equation, similar as for softwood glulam in EN 14080 [1], shall be derived.

Different to previous pioneering FEM models by Ehlbeck and Colling [6], Blaß et al. [7] and Frese and Blaß [8], the new model should consider later advanced modeling techniques and failure criteria, such as the use of the extended finite element method (XFEM) in conjunction with failure energies and a wider range of stochastic variables, which are taken into account to obtain better correlations between the simulations and experimental data. Emphasis is paid to the modulus of elasticity

(MOE) along board lengths and its proper description by an autocorrelation function. The computational model should allow the simulation of a wide range of geometries and size configurations, hereby capturing various aspects of the beam design such as the size effect, well. The model has to be calibrated with consistent sets of experimental data, including tension and bending tests with individual boards, with finger joints and full-sized glulam beams. This paper lays out the basic modelling approach as well as material calibration data and presents results of the ongoing research work.

2. Materials

A stochastic model for (bending) strength of glulam beams requires a good understanding and consistent experimental data of several mechanical properties of the individual boards used for the build-up and of the finger joints (glued multiple scarf-like connections) jointing the boards to laminations of beam length. The adhesive layers bonding the laminations to form the desired cross-sectional depth of the beam are not explicitly modelled and considered rigid.

A comprehensive database with this information has been obtained in the context of a European technical approval campaign [2], where a large set of oak (Querqus robur, Q. petraea) boards with origin from France were experimentally investigated at MPA University of Stuttgart, in both destructive and non-destructive manner. The boards (planed thickness: 20 mm) supplied by the approval holder, company Gamiz S.A., Spain, were visually classified according to DIN 4074-5 [9] as grades LS10 and LS13, the latter with some additional provisions. Further, glulam beams with widths of 100 mm and different cross-sectional depths of 200 mm and 300 mm were obtained, following termed *small* beams and *large* beams. The glulam beams of both sizes were built-up inhomogeneously, consisting of LS13 laminations at both outer zones (1/6) of cross-sectional depth h and LS10 laminations in the center $2h/3$. The length of the beams was 20 times the depth.

The material used to study the MOE variation along the board length in tension stemmed from a different batch of French oak, delivered by company Scierie Mutelet & Cie., France, in the context of the European research project, „EU Hardwoods". The boards had a cross-section of 27 mm × 160 mm, a total length of 2.4 m and conformed to non-structural grades QF2/QF3 according to EN 975-1 [10], re-graded into structural grades according to NF B 52-001-1 [11] at a later stage, not discussed here.

3. Experimental investigations

Tensile strength tests were performed with boards of both grades with and without finger joints, whereby the modulus of elasticity (MOE) was determined with reduced numbers, too (see Table 1).

Regarding the glulam beams, four-point bending tests according to EN 408 [12] were performed with 10 specimens each of both beam sizes. Prior to the bending tests of the beams, the distance between each adjacent finger joint in every layer was measured. Further, compressive strength and MOE tests parallel to the fiber were performed according to EN 408 [12], however exclusively for cross-sectional glulam dimensions of 100 mm × 120 mm.

To experimentally study the variation of the MOE along a single board, different methods can be applied: bending tests have proven to be a good option, as shown by Isaksson [13] and Aicher et al. [14], as well as dynamic tests, as performed by Colling and Scherberger [15]. However, for the specific application dealt in this paper, a direct measurement of the MOEs in a tensile test seemed to be more appropriate, as the failure-dominating loading mode is tension.

Each board was partitioned ideally outside the clamping areas into 15 *cells* of lengths equal to 100 mm, each of which was used to measure the MOE parallel to fiber and board's length direction by means of a specially modified extensometer, as shown in Fig. 1. Since only one of such extensometers was available, the test was repeated for each cell, and additionally for the whole board by extending the length of the extensometer. Finally, the board was loaded until failure and the failure position was allocated to one or more cells. Throughout the same differential load was applied. In total, 40 boards were tested with regard to local MOE distribution, global MOE and tensile strength.

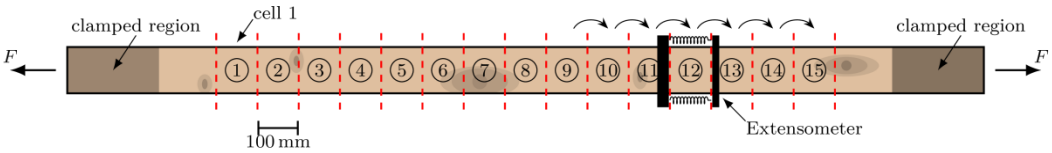

Fig. 1: Scheme for the determination of the MOE variation along a single board

4. Test results

Following, the tests results obtained with the boards and finger joints are specified. The test results with the beams are presented together with the simulation results in Table 3 in Section 7.

4.1 Global strengths and stiffnesses of boards and finger joints

All experimental data were evaluated statistically assuming a lognormal distribution, except for the variation of the MOE within a single board, where a normal distribution was chosen. The parameters obtained from this process are summarized in Table 1, giving the mean values, standard deviation and coefficient of variation (COV). It can be seen, that the visual classification of the boards in grades LS10 and LS13 indeed clearly separates the (unjointed) boards with regard to the mechanical properties MOE and tensile strength.

Regarding the finger joints, the tensile strengths, $f_{t,\mathrm{fj}}$, are rather equal for both grades, being mechanically sensible as raw density of both grades is very similar

and grade-determining defects, like knots and excessive fiber deviation, are not present in the jointed area. The mean values for $f_{t,\mathrm{fj}}$ were 44.6 MPa and 42.5 MPa for LS10 and LS13, respectively. Further, the COVs of LS10 and LS13 joints were very similar, with values of 22 % and 25 %, respectively.

Table 1: Statistical parameters of measured mechanical and dimensional properties of the boards and finger joints

Property	**distribution**	**N**	**mean**	**std.**	**unit**	**COV**
MOE (LS10)	lognorm	10	12711	1995	MPa	16 %
MOE (LS13)	lognorm	10	13434	3217	MPa	24 %
$f_{0,t}$ (LS10)	lognorm	50	45.1	14.4	MPa	32 %
$f_{0,t}$ (LS13)	lognorm	50	55.1	16.7	MPa	30 %
$f_{t,\mathrm{fj}}$ (LS10)	lognorm	50	44.6	10.0	MPa	22 %
$f_{t,\mathrm{fj}}$ (LS13)	lognorm	49	42.5	10.7	MPa	25 %
$f_{0,c}$ (LS10, LS13)	lognorm	14	50.1	0.046	MPa	5 %
ℓ_b (LS10, LS13)	lognorm	619	667.5	194.3	mm	29 %

The tensile strength results for the boards and finger joints indicate that in case of a lamination build-up by LS13 boards, the finger joints constitute doubtlessly the most probable failing point, as their tensile strength lays significantly (23 % on the mean level) below the tensile strength of the boards. This is one of the main issues with hardwood glulams, namely that finger joints exhibit lower strengths as compared to the wood of higher grade boards, a feature which is rarely observed in softwood glulams.

Table 1 also specifies the lengths of the boards, ℓ_b, i.e. the distance between two adjacent finger joints. The average length of 670 ± 190 mm is considerably lower as usually for boards in softwoods, where very roughly mean lengths in the range of 2.5 m to 3.5 m are usual. The very short board length, as compared to softwood glulam, results in a significantly higher number of finger joints and a strongly elevated influence of finger joints strength on the global beam capacity.

Also relevant for the analysis are the correlations between the different mechanical properties, such as MOE–$f_{0,t}$, MOE–$f_{0,c}$ and MOE–$f_{t,\mathrm{fj}}$. Since the amount of data available for the MOEs of each grade is small (N = 10), the correlations were calculated combining both grades. The results are presented in Table 2. As a consequence of the combination of the two grades, the correlations may not be totally representative for the dataset, but can be assumed as a reasonable approximation. The correlation between finger joint tensile strength and MOE, was based on the minimum MOE value of both jointed boards. As these data were not available for the regarded dataset, the specified correlation was taken from another dataset of French oak of similar characteristics, tested at FCBA, Bordeaux, within the EU Hardwoods project.

Table 2: Correlations between some mechanical properties of the oak boards (LS10+LS13)

	MOE	$f_{t,0}$	$f_{c,0}$	$\min(E_1; E_2)$	$f_{t,fj}$
MOE	1	0.81	0.81	–	–
$f_{t,0}$	0.81	1	0.9*	–	–
$f_{c,0}$	0.81	0.9*	1	–	–
$\min(E_1; E_2)$	–	–	–	1	0.8
$f_{t,fj}$	–	–	–	0.8	1

* values needed for the simulation, however, not experimentally derived.

4.2 MOE variation and strength correlation within board's length

Following, the intra-board MOE variation is discussed in preliminary manner as the evaluation is still on-going. For each of the 40 boards the MOE of every cell was calculated altogether with the global board MOE. Fig. 2a shows in an exemplary manner the variation of the cell MOE along two boards exhibiting rather different behavior, i.e. are rather moderate MOE variation (board No. 14) and a very expressed variation (No. 28). The COV in case of board No. 28 is 21 % and 5 % for the board No. 14. Further, the graph shows filled regions representing the failure location. It can be seen, that in one case (board No. 28) the failure occurs in the region of the lowest stiffness, whereas in the case of board No. 14 the failure is associated with a low stiffness, but not with the absolutely weakest cell. Fig. 2b shows the cumulative frequencies and the log-normally fitted distribution functions of the cell MOEs. As the grading of the boards is not yet finished, in the simulations a COV of 5 % was used for the cell MOE variation of the LS13 boards, whereas for the LS10 boards a value of 15 % was taken. The autocorrelation procedure of the adjacent cell MOEs with the respective global board MOE, assigned to the board in a first step, is discussed below.

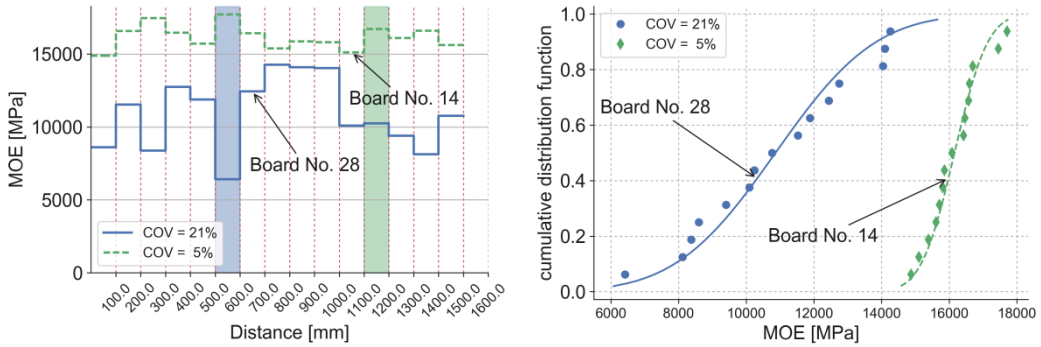

(a) (b)

Fig. 2: Variation of measured „cell" MOEs along length of two different boards. (a) discrete variations and tensile failure locations; (b) cumulative frequencies and fitted distributions

5. Generation of simulation input data

The statistical parameters obtained for the different properties of the laminations and finger joints were used to generate data for the boards for each simulated configuration. In doing this, special consideration was paid to the realization of the observed and fitted correlations between MOEs and strength values, as well as to the autocorrelation observed between the MOE values of the different cells within the same board.

5.1 Board properties at global level

The first part of the simulation process consists in generating a set of global mechanical properties for each lamination of the glulam build-up (see below). This means, that values for MOE, $f_{0,t}$ and $f_{0,c}$ are generated, starting from the respective known statistical distributions (see Table 1). These values are at the same time correlated between each other by means of the coefficients given in Table 2. The generation of data of individual distributions, e.g. $f_{t,0}$, is a trivial task, which can be solved by a number of statistical libraries with an implemented pseudo-random number generator. For this study, the statistical module of the Scipy python package [16] was used. The rather complex part of the problem is represented by the need to correlate the different random variables, which is done by means of the following algorithm:

1. samples of a normal distribution $\mathcal{N}(0,1)$ are independently generated for each of the random variables MOE, $f_{t,0}$ and $f_{c,0}$ and stored in separate columns in a matrix **R**.
2. Given the correlation matrix **C**, a matrix **U** is looked for, such that
$$\boldsymbol{U}^T\boldsymbol{U} = \boldsymbol{C}, \tag{1}$$
what is achieved by means of a square root decomposition. Other decompositions are also allowed, but may give slightly different results.
3. The set of correlated data, $\mathbf{R_c}$, is computed according to
$$\boldsymbol{R_c} = \boldsymbol{RU}, \tag{2}$$
which correspond to variables in the $\mathcal{N}(0,1)$ distributions.
4. To transform them into variables corresponding to the needed distributions of the mechanical properties, first the cumulative distribution function of these variables (in $\mathcal{N}(0,1)$) is computed. Using these values the percent point function of the desired distribution is calculated, which corresponds to the correlated sample of the needed distributions.

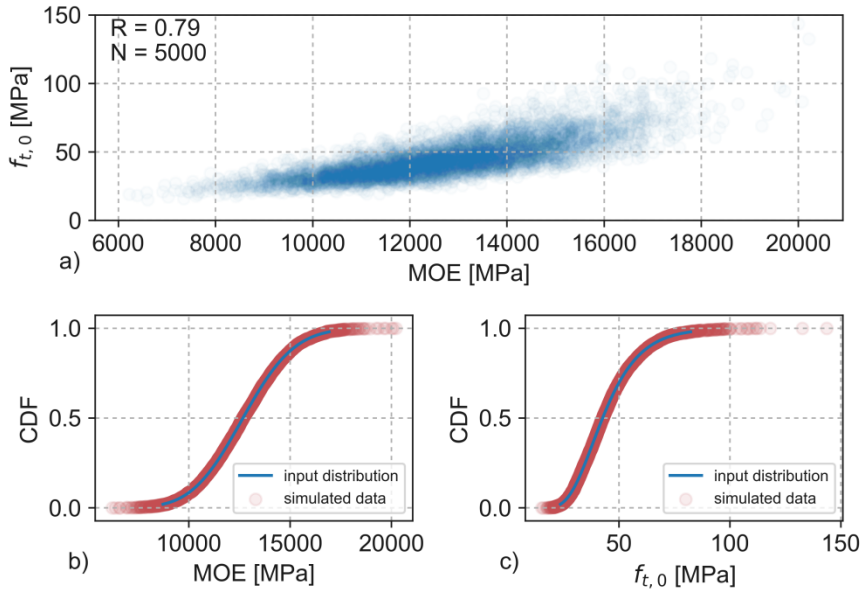

Fig. 3: Example of the correlated MOE – $f_{t,0}$ data generation; a) MOE–$f_{t,0}$; b, c) input distributions and simulations of individual properties MOE and $f_{t,0}$

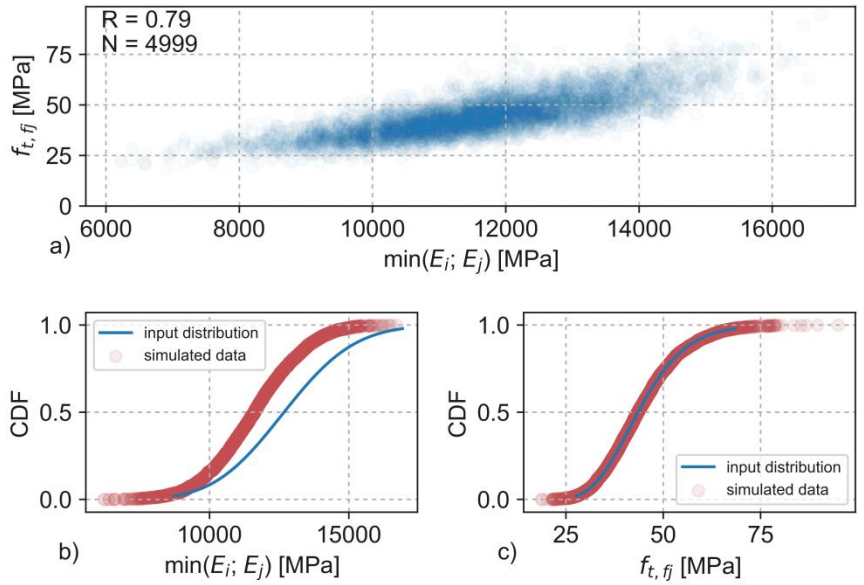

Fig. 4: Example of the correlated MOE – $f_{t,\mathrm{fj}}$ data generation. a) correlation between $f_{t,\mathrm{fj}}$ and $\min\{E_i; E_j\}$, b, c) input distributions and simulations of individual properties $\min\{E_i ; E_j\}$ and $f_{t,\mathrm{fj}}$

Fig. 3 shows an example of results for the MOE–$f_{t,0}$ correlation obtained with the described algorithm. It can be seen, that each of the variable samples (MOE and $f_{t,0}$) follows their corresponding distribution (blue lines in Figs. 4b, c), while maintaining a correlation of $R = 0.79$, which is very close to $R = 0.81$, given as the input (see Table 2). In addition, the needed number of board lengths is generated, which is done by simply taking a sample of random variates, corresponding to the *lognormal* distribution of the board lengths.

5.2 Finger joints – tensile strength and MOE

The procedure to generate the mechanical properties for the finger joints applies, in essence, the same method as for the generation of the properties of the individual boards, however, with a further step, as the data generated for the finger joints comprise two variables: MOE and $f_{t,\mathrm{fj}}$. The MOE of the finger joints is assumed to be correlated to the minimum of the two global moduli of elasticity $E_{ij,\min} = \min\{E_i; E_{j=i+1}\}$ of the jointed boards. A prerequisite for this is, of course, that the data corresponding to the boards have already been generated in a previous step, in a certain order, which needs to be respected. By order it is meant that the vector containing the values for the global MOEs has been defined, and thus, also the vector with the values for $E_{ij,\min}$, which will be referred to as $\mathbf{E}_{\mathrm{fj}}$. The problem is then to generate the correlated data for $f_{t,\mathrm{fj}}$ and $E_{ij,\min}$, where one of the vectors ($\mathbf{E}_{\mathrm{fj}}$) is given, which differs from the first method, where all the vectors of data were simultaneously generated.

If **E** and **P** are the vectors for MOE and $f_{t,\mathrm{fj}}$, respectively, which were randomly generated with the same procedure as explained in the previous Section, then the extra steps needed to order them consist in:

- obtaining the indices that sort $\mathbf{E}_{\mathrm{fj}}$ and name this resulting vector $\mathbf{I_j}$,
- then obtain the indices that sort **E** and name this vector $\mathbf{I_k}$,
- sort the vector **P** according to the indices $\mathbf{I_k}$, which will give a vector $\mathbf{P}^*$,
- and finally sort the vector $\mathbf{P}^*$ with the indices corresponding to $\mathbf{I_j}$, which will return the desired array of $\mathbf{f_{t,fj}}$.

The results obtained from this method will only be accurate if the size of the sample is large enough ($N \gtrsim 500$), which is guaranteed for these simulations, since the number of boards generated are in the order of thousands. An exemplary result can be observed in Fig. 4, where a total of $N = 4999$ finger joints were generated and successfully correlated to the vector $\mathbf{E}_{\mathrm{fj}}$, as can be seen from the correlation coefficient $R = 0.79$.

5.3 Autocorrelation of within-board property variation

An important point consists in the correct implementation of the variation of the different mechanical properties along each single board, as this has a fundamental influence on the so-called lamination effect. Specifically, the COV and autocorrelation coefficients need to be known, in order for the board to behave in a similar manner, as it would do in the reality. For the analyzed case, the COV was obtained experimentally, while for the autocorrelation between cells belonging to the same board, the following exponential law was assumed

$$p_i = exp(-d_i \cdot \alpha). \tag{3}$$

The parameter d_i represents the distance between the centroids of any pair of cells separated by i-times the constant length of the cells (in mm), while the factor α is a parameter that needs to be fitted. This simple law means that the closer two cells

are to each other, the larger the correlation between their respective mechanical properties will be. Since the data obtained from the experiments of intra-board MOE variation, are not fully evaluated, preliminary a value of α = 0.01 was assumed. This assumption delivers e.g. for three adjacent cells p_i values of $p_1 = 0.37$, $p_2 = 0.14$ and $p_3 = 0.05$,

To generate the autocorrelated set of data, an autoregressive (AR) model process of order equal to the number of cells to be generated was used. The coefficients for the autoregressive *lag*-polynomial were calculated for each board by

$$\boldsymbol{p} = [1 \quad p_1 \quad p_2 \quad \dots \quad p_{n-1}] \tag{4}$$

where n is the number of cells of any given board.

Finally, the values generated for one board are shifted to meet the following conditions: 1) for the MOEs, the values are shifted so that the mean of the generated data corresponds to the value of the global MOE for the lamination; and 2) for the tensile and compressive strengths, the values are shifted in such a manner that the minimum of the generated data equals the global $f_{t,0}$ or $f_{c,0}$ of the board, respectively. It is also worth mentioning, that it is assumed that the MOE, $f_{c,0}$ and $f_{t,0}$ vary with a ratio 1:1:1 along the board, i.e. if the MOE goes down in the next cell, so do $f_{t,0}$ and $f_{c,0}$, too, all following their respective distributions. An example of data generated with this method is shown in Fig. 5a, where values for the „cell" MOEs were generated for COVs of 5 % and 20 %. Fig. 5b depicts the cumulative frequencies and the distribution functions of both generated sets.

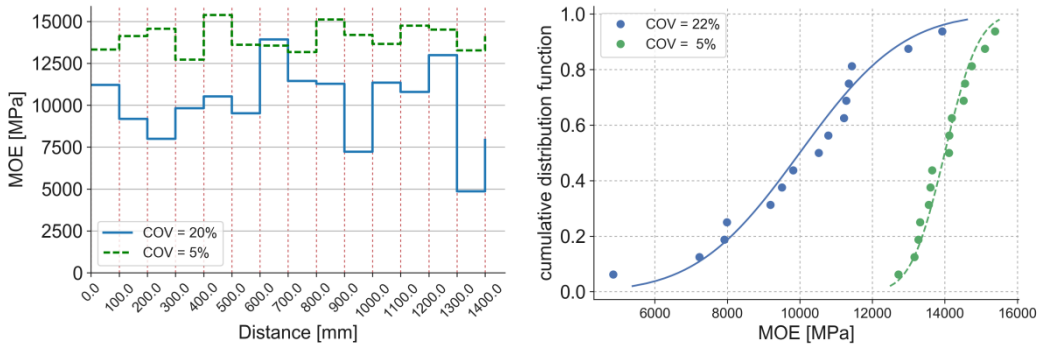

a) b)

Fig. 5: Variation of simulated „cell" MOEs along the length of two different boards, a) discrete variations, b) cumulative frequencies and fitted distributions

6. Finite element model

6.1 General and fracture energies

The aim of the developed finite element (FEM) model is to reproduce the beam properties and the applied bending strength test conditions (EN 408 [12]), hence allowing a direct comparison with the experimental results obtained for the oak glulam beams. Similar FEM models have been developed for softwood glulams

first by Ehlbeck and Colling [6] in the 1980's, establishing the so-called „Karlsruhe model", then refined by Blaß et al. [7]. The latter results served as a basis for the current design equation for the bending strength of glulam beams made from softwoods, implemented somewhat modified in EN 14080 [1]. The basic features of the „Karlsruhe model" were then extended to hardwood glulam made of beech wood by Blaß et al. [7] and Frese [17]. More recently, new numerical models have been developed, introducing new parameters like variable lengths of boards (Fink [18]), or, very fundamentally, the inclusion of fracture energies of the wood material by Blank et al. [19].

The here presented two-dimensional model applies many of the concepts specified in the above cited literature, however comprises new relevant parameters and modelling techniques, such as the extended finite element method (XFEM). The latter addition has a strong potential of increasing the accuracy of the simulation model, since it describes the failure as a process, where several cracks may start independently, stop and continue before global failure is reached.

Two-dimensional, linear plain stress elements with reduced integration (CPS4R) were used for the beam modelling and rigid line elements (R2D2) were applied in the support and loading zones. The modelling was performed with Abaqus 2016.

The essential global mechanical properties used for the model are those specified in Table 1. The properties not given in Table 1, such as MOE perpendicular to the fiber (E_y) and shear modulus (G_{xy}), were chosen according to EN 338 [20], dependent on the MOE parallel to fiber attributed to the boards in stochastic manner.

Different fracture energies were assigned to finger joints and boards. For the finger joints, a mixed-mode $G_{f,\mathrm{fj}}$ value of 5 N/mm (5×10^3 J/m^2) was first tried. This value was obtained based on the investigations by Serrano [21] and Stapf [22], and normalized by the true length of the finger joint surface, as shown in Fig. 6. This energy value lead to rather low values for the bending strengths in preliminary simulations, being the reason why a higher value of 10 N/mm was finally used. For the boards, a fracture energy of 20 N/mm ($2 \times 10^4\ J/m^2$) was assigned, which is the value forwarding satisfactory results in the model. Blank et al. [19] used a unique fracture energy $G_f = 10\ N/mm$ for both wood and finger joints. The applied values lay in a physically sensible range but are undoubtedly inversely calibrated, and will be further investigated. The failure criterion chosen corresponds to the *maximum stress criterion*, where damage initiation is related to the tensile strength of either the finger joint or the board.

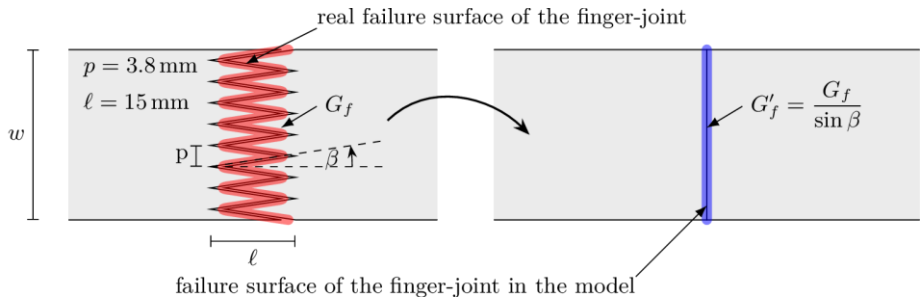

Fig. 6: Real failure surface of a finger joint, assuming it fails along the bond line (left), and failure area in the model (right). The fracture energy G_f has to be modified accordingly, so that the total energy released in the real finger joint and in the model are equal.

6.2 Hierarchical model levels

In the model, the beam is represented through various hierarchical/scale levels, which define the properties of the beam as a whole. Proceeding from the highest to the lowest level, the model defines first the entire inhomogeneous beam, subdivided into three parts, representing the outer zones ($2 \times 1/6$) and the inner one ($2/3$), as can be seen by the different colors in Fig. 7. At this level, the different statistical parameters corresponding to LS10 (inner zone) and LS13 (outer zones) are assigned to each part, respectively. The next level corresponds to the sets of boards which compose each of these three parts. The boards are connected at their ends by finger joints, which are represented in the model as areas of 20 mm (= lamination thickness) × 40 mm with their respective material properties. Finally, each board is subdivided into *cells* of 100 mm length to represent the variation of the mechanical properties within the board. Each of these cells is meshed with rectangular elements with edge lengths of 1/3 of the thickness of the lamination, i. e. ~7 mm.

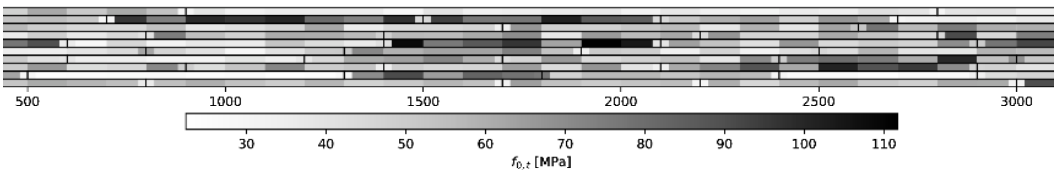

Fig. 7: Example of FEM model of inhomogeneous beam build-up, where the different levels of the model can be observed along with the variation of the tensile strength. The two outer laminations at the top and the bottom of the beam correspond to LS13 boards, while the rest of the laminations represent LS10 boards. The difference in the intensity of the color depicts the variation of the property (lighter zones mean lower values and darker zones indicate larger values).

The calculations reported here were done for two different glulam depths, 200 mm and 300 mm, investigated experimentally. Both glulam depths correspond to build-ups with 10 and 15 laminations with thicknesses $t = 20\ mm$, respectively (see Section 2). For each one of both sizes 100 simulations were performed, actually not

being much for a Montecarlo simulation, but assumed/proven to deliver sufficiently accurate results.

6.3 Realization of boundary conditions

As the model aims at damage evolution and ultimate load prediction, appropriate boundary conditions have to be provided to guarantee the stability of the system during the solving process. The first step concerns the application of the load. Since direct application of the load at points RP3 and RP4 (see Fig. 8) would lead to system instability, displacement controlled application of the load is necessary. However, due to the random distribution of MOEs in the glulam beam, the application of vertical displacements at the reference load application points RP3 and RP4 would lead to an unequal distribution of the forces at both loading points, not representing the real test situation. A common solution [8], [17] to overcome this effect is to model a truss-like structure, which connects both points to a third one (here RP5), which is then loaded displacement-controlled in vertical direction. This approach was further simplified in the model by the introduction of a linear equation that relates the vertical displacements v_i $(i = 3, 4, 5)$ of the reference points RP3, RP4 and RP5 by

$$v_5 - 0.5 \cdot (v_3 + v_4) = 0, \tag{5}$$

ensuring that the reaction forces at points RP3 and RP4 remain equal throughout the simulation.

The second condition couples the support locations RP1 and RP2 (Fig. 8) in the horizontal direction in order to prevent uncontrolled horizontal displacements in the failure state. This is achieved by forcing the horizontal displacements u_1 and u_2 to be always of the same magnitude but in the opposite direction:

$$u_1 + u_2 = 0. \tag{6}$$

The reference points RP1 and RP2 are attached to one-dimensional rigid elements (R2D2), arranged vertically with a length equal to the depth of the beam, then connected to the vertical edges of the beam by means of *tie constraints*. Similarly, rigid line elements are placed horizontally at the reference points RP3 and RP4 with a load/displacement application length of 1/3 of beam depth.

In order to adequately capture the failure evolution of the beam, an element-enriched region was defined in the bending-tension area of the constant moment zone, enlarged at both ends by an extra length of 1/9 of the beam's length, to account for a possible failure outside of the constant moment region (see Fig. 8).

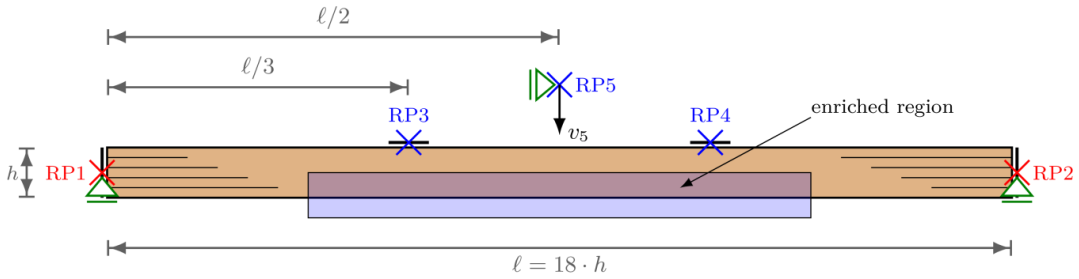

Fig. 8: Finite element model – geometry, enriched element region and boundary conditions

7. Simulation results

7.1 Damage and stiffness evolution

For each simulation, the reaction forces at points RP1 to RP4 and the vertical displacement at RP5 were extracted to calculate the bending stresses of each specimen. Ultimate load F_u was determined as the load prior to the first force drop-off >10 % irrespective of the fact that in very rare cases an even somewhat higher load, at rather large deflection occurred.

Fig. 9a reveals the stiffness evolution of the beam discussed above in terms of engineering (not local FEM) bending stress $\sigma_m = F\ell/(wh^2)$ vs. vertical displacement at RP5. The graph depicts small, discrete stiffness changes in the pre-peak load range. For comparison, Fig. 9b shows a rather different damage scenario of another simulated beam, with increasing non-linearity beyond $\sigma_m = 40$ MPa due to progressive damage in tension and plasticity in the compression zone.

Fig. 10 shows exemplarily for a beam with cross-section of 100 mm × 200 mm the bending stress distribution at two different load levels. In detail, Fig. 10a which depicts the stress state at $0.75F_u$ in the constant moment area and slightly beyond, reveals a clear asymmetry in the stress distribution due to the stochastic variation of the MOEs in each board. It further shows the crack initiation point of the first crack, which, however, did not lead to global failure. Fig. 10b shows the ultimate load state, together with the relevant failure crack, which is at a different location as compared to Fig. 10a. Additionally, Fig. 10b presents the location of every finger joint (red regions) of the glulam beam, revealing that the crack-determining ultimate load started in the region of a finger joint. Fig. 10c shows a detail of the failure region, where the finite element mesh can also be recognized. Some other cracks seen in the vicinity of the failure zone were not decisive for the beam's moment capacity.

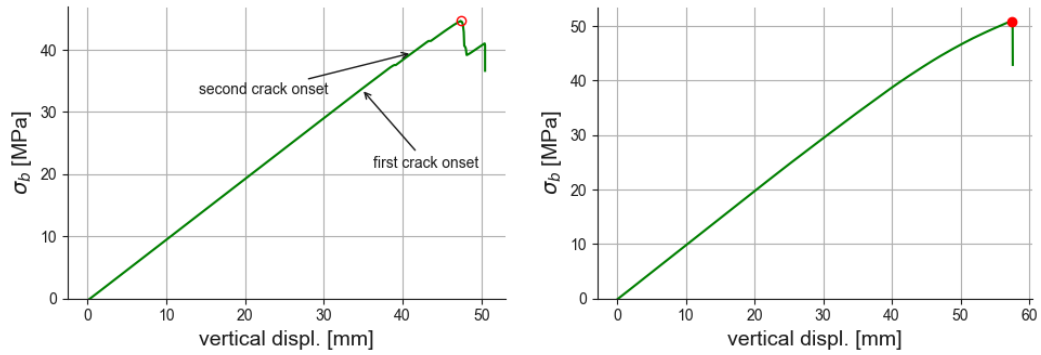

(a) (b)

Fig. 9: Bending stress in constant moment area vs. vertical displacement at RP5 at increasing loading for two simulated glulam beams. a) brittle failure evolution; b) ductile failure evolution

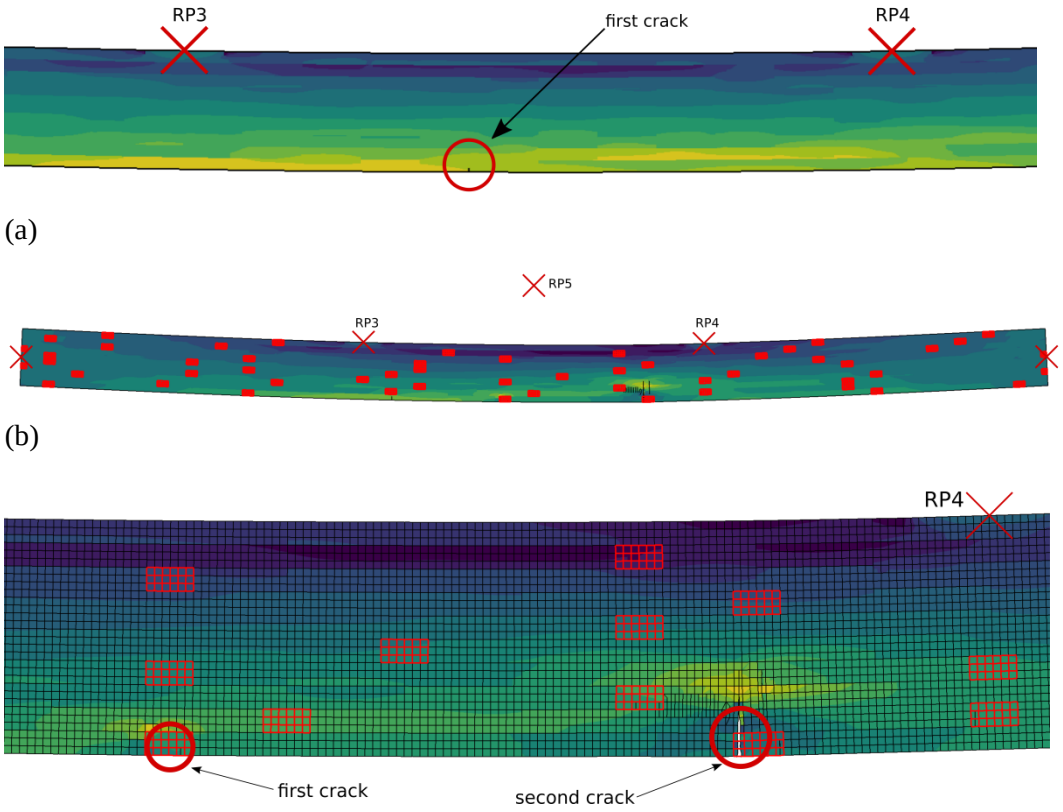

(a)

(b)

(c)

Fig. 10: Bending stresses in a simulated glulam beam (see Fig. 9a); a) $F \approx 0.75F_u$, first crack onset; b) $F = F_u$, second crack has fully developed (red squares = location of all finger joints); c) detail of crack areas

7.2 Size effect and comparison with test results

A comparison of the experimental and simulated results is presented in Fig. 11 for both analyzed beam sizes. Fig. 11a shows the experimental and calculated cumulative frequencies of bending strengths, and Fig. 11b depicts the lognormal cumulative distributions fits. The graphs reveal for both beam sizes a very good agreement

of experiments and simulations. In this context it is important to underline that the model successfully captures the decrease in bending strength for larger cross-sectional depths, widely known as the size effect in glulam beams.

Table 3 specifies with regard to a detailed quantitative comparison of experiments and simulations the statistical parameters –mean value, 5% quantile and COV– of the tested and calculated samples. The deviations on the mean bending strength level are 1.2 % and 1.6 % for the small and large beams, respectively, and very similar, 2.5 % (small beams) and 0.3 % (large beams) on the 5 % quantile strength level. Further, the COVs are in good agreement.

Table 3: Bending strengths of oak glulam beams according to tests and XFEM simulations

Cross-section (width × depth) (mm × mm)	Beam bending strengths [MPa]					
	Test results			Simulation results		
	mean	5 % quant.	COV	mean	5 % quant.	COV
100 × 200 (10 lam)	47.8	39.9	10.1%	47.2	38.9	11.3%
100 × 300 (15 lam)	43.4	36.4	10.4%	44.1	36.5	11.1%

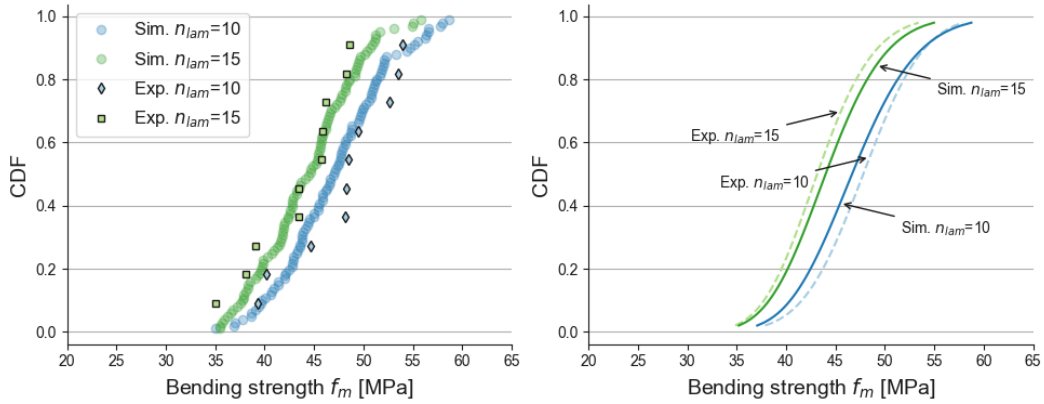

Fig. 11: Experimental and XFEM calculated results of bending strengths of oak beams with two different sizes, a) Cumulative frequencies; b) fitted lognormal distributions

8. Conclusions

The reported investigations revealed that a simulation prediction of load capacities, and hence of bending strength of inhomogeneously built-up glulam beams made of hardwood species oak, is well possible and in very accurate agreement with experimental data. Noteworthy is, that the size effect is captured precisely. In an extension of previous well-established FEM models for the numerical analysis of bending strength of softwood glulams, now the XFEM method was applied. This approach is especially apt to capture the damage evolution and cracking in heterogeneous materials. The load capacity prediction depends decisively on the fracture energies for the wood and finger joints and on the autocorrelation of moduli of elasticity, varying grade-dependent pronouncedly along the length of the boards. Further simulation runs with the model, based on different input values for boards,

finger joints and calibration data for beams, will enable a parametric closed-form hardwood glulam bending strength equation similar to the present EN 14080 [1] solution for softwood glulams. As hardwood boards are often considerably shorter as compared to softwoods, resulting in a pronounced increase of finger joints, the design equation might include a parameter referencing the length of the boards. Due to the extreme heterogeneity of hardwoods, solutions restricted to defined density ranges, grades and species groups might turn out to be sensible in order to limit the error of the deduced equation parameters.

9. Acknowledgements

The financial support by FNR, Fachagentur Nachwachsende Rohstoffe e. V. contract 22004014, within the European ERA-WoodWisdom project "European hardwoods for the building sector (EU Hardwoods)" is gratefully acknowledged. Many thanks are owed to the German association of glulam manufacturers for co-funding the project.

10. References

[1] EN 14080:2013 *Timber structures – Glued laminated timber and glued solid timber* – Requirements.

[2] ETA-13/0642:2013 European Technical Approval, *VIGAM – Glued laminated timber of oak.*

[3] Z-9.1-821:2013 *Zulassungsgegenstand: Holz Schiller Eiche-Pfosten-Riegel-Brettschichtholz*. Antragsteller: Holz Schiller GmbH, Regen.

[4] ETA-13/0646:2013 European Technical Approval, *SIEROLAM – Glued laminated timber of chestnut*.

[5] Aicher, S., Stapf, G. (2014) *Glulam from European white oak: finger joint influence on bending size effect*. Materials and Joints in Timber Structures, RILEM Bookseries 9:641-656, Springer.

[6] Ehlbeck, J., Colling, F. (1987) *Biegefestigkeit von Brettschichtholz in Abhängigkeit von Rohdichte, Elastizitätsmodul, Ästigkeit und Keilzinkung der Lamellen, der Lage der Keilzinkung sowie von der Trägerhöhe*, Holz Roh und Werkstoff, 45: 95–99.

[7] Blaß, H.J., Frese, M., Glos, P., Linsenmann, P., Denzler, J. (2005) *Biegefestigkeit von Brettschichtholz aus Buche,* Karlsruher Berichte zum Ingenieurholzbau; 1, Universitätsverlag Karlsruhe.

[8] Blaß, H.J., Frese, M., Denzler, J.K., Linsenmann, P., Ranta-Manus, A. (2009) *Zuverlässigkeit von Fichten-Brettschichtholz mit modifiziertem Aufbau*. Karlsruher Berichte zum Ingenieurholzbau; 11, Universitätsverlag Karlsruhe.

[9] DIN 4074-5:2008 *Strength grading of wood – Part 5: Sawn hardwood*.

[10] EN 975-1:2011 *Sawn timber – Appearance grading of hardwoods – Part 1: Oak and beech*.

[11] NF B 52-001-1:2011 *Classement visuel pour l'emploi en structures des bois sciés français résineux et feuillus*.

[12] EN 408:2012 *Timber structures – Structural timber and glued laminated timber – Determination of some physical and mechanical properties*.

[13] Isaksson, T. (1999) *Modelling the variability of bending strength in structural timber – length and load configuration effect*, PhD thesis, Report TVBK-1015, Lund Institute of Technology, Lund, Sweden.

[14] Aicher, S., Höfflin, L., Behrens, W. (2002) *Determination of local and global modulus of elasticity in wooden boards*. Otto-Graf-Journal 13, MPA University of Stuttgart.

[15] Colling, F., Scherberger, M. (1987) D*ie Streuung des Elastizitätsmoduls in Brettlängsrichtung*. Holz Roh und Werkstoff, 45: 95–99.

[16] Jones, E., Oliphant, T., Peterson, P., others (2001) SciPy: *Open source scientific tools for Python*.

[17] Frese, M., Blaß, H.J. (2007) *Characteristic bending strength of beech glulam*. Materials and structures, 40(1): 3–13.

[18] Fink, G. (2014) I*nfluence of varying material properties on the load-bearing capacity of glued laminated timber*. PhD thesis, No. 21746, ETH Zürich, Switzerland.

[19] Blank, L., Fink, G., Jockwer, R., Frangi, A. (2017) *Quasi-brittle fracture and size effect of glued laminated timber beams*. European Journal of Wood and Wood Products:1–15 (published online on 17 February 2017).

[20] EN 338:2016 *Strength classes*.

[21] Serrano, E. (1997) *Finger-joints for laminated beams. Experimental and numerical studies of mechanical behavior*. Report TVSM-3021, Division of Structural Mechanics, Lund University, Sweden.

[22] Stapf, G. (2010) *Energiedissipationsfähigkeit und Ermüdungsverhalten von geklebten Holzverbindungen*, Master thesis, University of Kassel.